GEOPHYSICS

Alkaline vents recreated in two dimensions to study pH gradients, precipitation morphology, and molecule accumulation

Maximilian Weingart[1], Siyu Chen[2], Clara Donat[3], Vanessa Helmbrecht[4], William D. Orsi[4,5], Dieter Braun[1], Karen Alim[3,2]*

Alkaline vents (AVs) are hypothesized to have been a setting for the emergence of life, by creating strong gradients across inorganic membranes within chimney structures. In the past, three-dimensional chimney structures were formed under laboratory conditions; however, no in situ visualization or testing of the gradients was possible. We develop a quasi–two-dimensional microfluidic model of AVs that allows spatiotemporal visualization of mineral precipitation in low-volume experiments. Upon injection of an alkaline fluid into an acidic, iron-rich solution, we observe a diverse set of precipitation morphologies, mainly controlled by flow rate and ion concentration. Using microscope imaging and pH-dependent dyes, we show that finger-like precipitates can facilitate formation and maintenance of microscale pH gradients and accumulation of dispersed particles in confined geometries. Our findings establish a model to investigate the potential of gradients across a semipermeable boundary for early compartmentalization, accumulation, and chemical reactions at the origins of life.

INTRODUCTION

Investigating the origins of life necessarily leads to the question of which possible locations could have provided promising conditions for the emergence of living systems on a prebiotic Earth. One of the theories today focuses on alkaline vents (AVs) as a promising setting, providing unique chemical and geophysical conditions (*1*–*4*). AVs on the prebiotic seafloor are predicted to have formed chimney structures, where warm alkaline fluids were exhaled into an acidic ocean enriched in dissolved iron(II) (*5*, *6*). Upon contact of the fluids, highly reactive Fe(Ni)S minerals precipitate and enclose the alkaline fluid stream to form a tubular network that grows into chimney-like structures (*3*, *7*). The precipitate thereby acts as a permeable mineral membrane (*8*–*10*) that allows for the generation of steep gradients in pH, redox potential, and temperature, thus providing not only the nonequilibria that might have been crucial for the emergence of life (*11*–*13*) but also a potential energy source for early life forms (*2*, *9*). The mineral surfaces, at the same time, could serve as a catalytic site for abiotic organic synthesis reactions (*7*, *14*), while the inflowing water would provide a constant source of chemical nourishment (*2*). As shown in recent work (*15*), vent minerals could have also facilitated the localization and accumulation of dissolved RNA molecules. The physical nonequilibrium conditions provided by temperature gradients between the fluids can further boost accumulation of dissolved species and increase their local concentration manifold (*16*, *17*). The combination of those characteristics makes AVs also a very interesting location for inorganic catalytic reactions, polymerization or replication (*11*, *18*–*20*). On the other hand, the gradients in pH, separated by a semipermeable membrane, could have worked as an electrochemical reactor, providing a precursor setting for modern autotrophic cells (*1*–*3*, *8*, *21*), although recent publications showed only low yields of simple organic products (*21*–*23*). Which of the conditions provided by AVs, however, are critical or sufficient to drive molecular evolution at the origins of life is mostly unknown.

A well-studied example of AVs formed at moderate temperatures is the Lost City hydrothermal field near the mid-Atlantic spreading centers (*24*, *25*). In general, these vents emerge when ocean water percolates into cracks and fractures of Earth's upper mantle, which typically comprises minerals of ultramafic rock. Upon contact with water, a metamorphic chemical reaction (serpentinization) converts the ultramafic rock to serpentinite (*14*, *26*). The serpentinization-dominated system vents alkaline fluids at ambient temperatures, coprecipitating mainly calcium carbonates and brucite upon mixing with seawater (*24*). However, compared to modern oceans, prebiotic oceans of the Hadean and Archean were likely more acidic (*1*, *27*, *28*), due to saturation with CO_2 from the atmosphere (*8*) and ferruginous, i.e., anoxic conditions with high concentrations of dissolved iron (*5*, *8*, *29*). The acidity of prebiotic seawater (*1*) probably prevented the crystallization of acid-soluble minerals, like the characteristic minerals of Lost City (*25*). Therefore, Lost City–type chimneys were most certainly not present on early Earth; however, serpentinization and the overall mechanism were likely prevalent, particularly since ultramafic intrusions could have been more frequent (*6*), probably even more abundant. Experimental recreations of Hadean ocean chemistry and AVs have demonstrated the capacity for iron oxide and iron sulfide minerals in AV chimneys to accumulate nucleic acids including RNA (*30*). Notably, highly reactive surfaces of ferromagnesian phyllosilicates, especially at AVs, were found to concentrate nucleic acids or nucleotides by adsorption, which could save them from dilution in the prebiotic ocean (*31*). Moreover, "white and green rust"

[1]Systems Biophysics and Center for NanoScience (CeNS), Ludwig-Maximilians University Munich, Amalienstraße 54, 80799 München, Germany. [2]Max Planck Institute for Dynamics and Self-Organization, Am Faßberg 17, 37077 Göttingen, Germany. [3]TUM School of Natural Sciences, Department of Bioscience; Center for Protein Assemblies (CPA), Technical University of Munich, Ernst-Otto-Fischer-Str. 8, 85748 Garching b. München, Germany. [4]Department of Earth and Environmental Sciences, Ludwig-Maximilians University Munich, Richard-Wagner Straße 10, 80333 München, Germany. [5]GeoBio-CenterLMU, Ludwig-Maximilians University Munich, Richard-Wagner Straße 10, 80333 München, Germany.
*Corresponding author. Email: k.alim@tum.de

(amakinite and fourgerite) ferrous-ferric oxyhydroxide minerals that precipitate during the growth of chimneys in AVs under ferruginous conditions have been found to concentrate RNA within the chimney structure from surrounding ferruginous solution (*15*). This experimental results reflect the naturally occurring mineralogy of AV systems, where amakinite or "white rust" (the rare ferrous analog of brucite) was detected in the basement rocks below the Lost City hydrothermal field (*32*, *33*). In addition to iron oxyhydroxides, iron sulfide minerals also promote the RNA complexation concentration within AV hydrothermal chimney structures (*34*). NASA undertook several studies to recreate the conditions of prebiotic AVs in the laboratory but has so far only investigated the structures in three dimensions (*13*, *23*, *35*, *36*).

Controlled precipitation reactions have a long history, reaching back to early alchemists, and are now comprised in the field of chemobrionics (*37*). The resulting structures, often referred to as chemical gardens, can be seen as a simple example of self-organizing systems that exhibit all kinds of different morphologies under different chemical and physical conditions (*37*, *38*). Apart from precipitation and crystallization, structure growth is driven by fluid advection through either active injection (*39*–*42*) or osmosis and convection (*43*, *44*). In the past years, they have also been increasingly studied in quasi–two-dimensional (2D) settings using microfluidic devices like Hele-Shaw flow cells (*10*, *40*, *45*, *46*). The focus is not only mostly on reaction parameters that allow ordered structures like hollow cylinders but also on mathematical modeling of the resulting patterns (*39*, *46*, *47*). Because of their apparent similarity to living organisms (*37*), there was huge interest in chemical garden structures in the early stages of the origins of life field (*38*, *48*), but had been neglected since, until NASA researchers started to recreate hydrothermal vent analogs in the laboratory (*23*, *35*). However, so far, none of the chemical garden studies in confined geometries has attempted to recreate the conditions of the origins of life on Earth.

In our experiments, we use a thin, translucent microfluidic cell built up by a cutout from a Teflon sheet that is sandwiched between two sapphire slides and located horizontally on the stage of a microscope. The rectangular chamber is filled with an acidic iron solution to simulate the ocean, and a sodium hydroxide solution injected by a syringe pump simulates the venting of alkaline fluid (see Fig. 1). This setup of the flow cell allows for microscope imaging in bright-field and dark-field mode. Although the thin mineral membranes formed in hydrothermal vents have been studied in microfluidics before (*9*, *21*, *49*–*51*), only controlled single membranes were created by laminar coflow of the fluids. Our experiments, here, are designed to provide a 2D representation of the 3D physiology of AVs, where acidic and alkaline fluids come into contact.

Here, we show that our setup enables us to visualize the formation of pH gradients in a quasi-2D model of alkaline vents to study the effects of physical parameters like flow rate and fluid concentration on resulting morphologies and emerging gradients. Our results show that finger-like precipitation patterns at mediate flow and concentration facilitate the formation of pH gradients while at the same time allowing for the accumulation of dispersed particles on the reactive mineral surfaces. The confined microfluidic chamber can therefore be seen not only as a model for the geological analog but also as a simulation of potential mixing of the fluids that could already start in the cracks and fractures of the seafloor even before the alkaline fluid is vented into the ocean. Our setup therefore provides a way to simulate chemicophysical hydrothermal vent experiments in the laboratory in low volume.

RESULTS

To mimic mineral precipitation in hydrothermal vents, we used a custom-built microfluidic flow cell to inject alkaline fluids into acidic ocean water (fig. S1). This, on the one hand, enables us to get a spatiotemporal visualization of the resulting morphologies and, on the other hand, also serves as a model for potential precipitation processes already starting in the narrow rock pores in the seafloor. The microfluidic chamber of 500 μm thickness is prefilled with an acidic, iron-containing ocean analog, in which the alkaline fluid is injected at a constant flow rate using a high-precision syringe pump. Gradients and morphologies can be visualized with the aid of pH-sensitive dyes immersed into both fluids.

Variation of pH and flow rate

We found that the physical parameters influencing the resulting morphology are mainly flow rate and the alkalinity (i.e., the concentration) of the inflowing sodium hydroxide solution. By variation of these two parameters, we defined boundaries for each regime at which the final morphology is not altered by further changes in one of the parameters. The influence of flow rates and concentrations on the resulting morphologies is visualized using a universal pH indicator. The steady-state images, in which further inflow does not alter the morphology any more, are shown in Fig. 2. Different inflow rates of 2.0 to 10.0 ml $hour^{-1}$ and alkaline concentrations from 0.2 to 1.0 M result in a diverse set of morphologies, from which three dominant structural patterns can be identified: "layers/rings," "precipitation fingers," and "flow fields." Flow fields form as large almost homogeneous areas of both fluids due to weak precipitation at low flow rate and/or low inflow concentrations, whereas layers and rings emerge as thick layered precipitates completely excluding the ocean fluid at high flow and strongly alkaline pH. In between the limits of both regimes, we observe precipitation fingers as parallel structures that maintain stable precipitation patterns. Higher concentrations of in-flowing sodium hydroxide, together with high flow rates, result in faster precipitation and stronger precipitate formation. The motion of the fluid flow entering the chamber is purely advection driven. Lowering flow and/or influx concentration further the initial motion gets increasingly diffusion governed. Therefore, the diffusive fields takes the longest time to reach the steady state since, even after complete filling of the chamber, intermixing of the fluids still continues via diffusion across the weak precipitate structures.

Time-dependent morphology formation

Variation of flow rate and concentration of the injected fluid showed that the three dominant morphologies emerge on different subsequent timescales. An even clearer visualization can be seen in Fig. 3, where the alkaline areas for each of the three morphologies are highlighted by a pH-dependent fluorescent dye [2′,7′-bis-(2-carboxyethyl)-5-(and-6)-carboxyfluorescein (BCECF)]. Among these three time-dependent patterns, layers/rings form within the first 10 to 15 s and fill up the complete chamber. For the mid-regime, initially thick layered precipitates grow until around 30 s, at which point the bulk flow is divided into multiple smaller flow trajectories that form the characteristic precipitation fingers. With

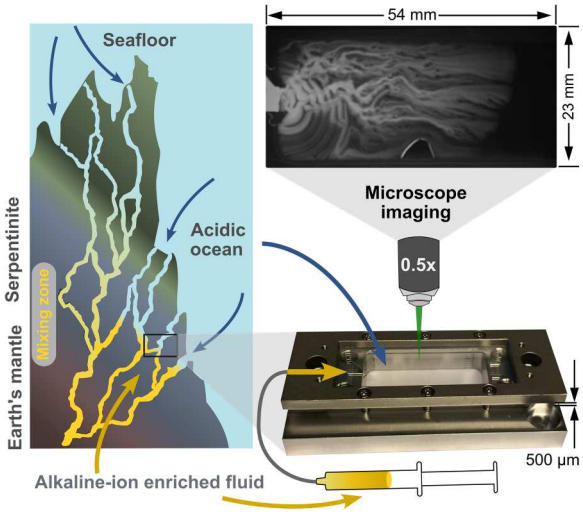

Fig. 1. Mixing of alkaline and acidic solutions in seafloor rock pores is mimicked in a microfluidic flow cell. Acidic ocean water percolates the narrow cracks and pores of the seafloor and is converted to an ion-enriched and strongly alkaline fluid by interaction with the surrounding rock. When this fluid is exhaled back into the ocean, rapid mineral precipitation happens upon contact with the ocean water. To mimic this scenario in the laboratory, an alkaline sodium-hydroxide solution is pumped at a controlled flow rate into a flat microfluidic chamber prefilled with an acidic iron solution. Microscope imaging with pH-dependent dyes allows the visualization of different morphologies, depending on inflow rate and OH^- concentration, and the assessment of emerging pH gradients.

increasing time, these precipitations get weaker and the fingers start to diffuse out perpendicularly to the flow direction until the top end of the chamber is reached. Similarly, in experiments revealing flow fields as dominating morphology, we observe the shaping of weak and thin finger-like precipitates within the first 120 s until the diffusive structure of the homogeneous flow fields dominates, due to mitigating precipitation. By varying OH^- ion concentration and inflow rate, we can control the timescales for the mineral precipitation pattern formation. The formation timescale gets longer for each of the dominating patterns and ranges from a few seconds (layers/rings) over 1 to 2 min (precipitation fingers) to above 3 min (flow fields), where no stable steady state could be observed within the measurement time. Comparing all three experiments, which exhibit one dominant morphology each (see Fig. 3), we can assess that the overall vent formation also scales over time.

pH-dependent dye and fluid flow

Apart from mapping the areas of different pH, the fluorescent dye also allows the tracing of flow and ion interchange over time (see Fig. 3). This is essential for the observation of two major features: gradient formation and their subsequent maintenance after entering the morphological steady state. Especially in the layers/rings, it can be seen that over time a main flow dominates through the center of the thick layers, leading to fading intensity of the fluorescent dye in the areas farther outside. This indicates a decrease in pH most likely due to ionic interchanges between the fluid and the mineral precipitates. However, this effect cannot be observed in the precipitation fingers as the flow is not bypassing earlier formed structures but rather divides into the smaller subflows forming the characteristic finger structures. The constant ion inflow maintains the fluorescence and, hence, the pH gradients even after reaching the steady state. The flow fields, on the other hand, show fading of the fluorescent dye by diffusing into the remaining ocean liquid due to weak and unstable mineral structures. This happens even though a similar subflow division as for the precipitation fingers can be seen in the beginning (Fig. 3). Because of this ongoing mixing of the two fluids by diffusion, all initially emerging gradients are equilibrating in the flow field morphology.

Potential for gradient formation

The potential of each morphology for the formation of gradients can be assessed from the final vent morphology of each time evolution in Fig. 3. The layer/ring structure does not allow for any gradients to form between alkaline fluid and acidic ocean analog, since all of the acidic liquid in the chamber is either consumed in precipitation or depleted from the chamber as it fills up with precipitate and alkaline solution. The only possible gradients would be the ones between shortcut flow and areas of fading pH as described above. However, those gradients would not be maintained and separated by a mineral membrane and thus equilibrate quickly by diffusion. This effect is shown in the plot of a cross-section through the chamber over time plot (Fig. 3C, right): The width of the blue (alkaline) areas decreases, as the fluorescence of the outer areas is depleted and a main flow forms. The same is valid for the flow field structures, since no steady state can be reached within the time of the experiment such that the fluids keep intermixing through the weak membranes forming between 30 and 200 s. Thus, the pH is equilibrating gradually, which can be seen by the faint edges of the precipitates in the dark-field images and the widening width of blue/white (alkaline) areas in the cross-section over time plot (Fig. 3A, right). In contrast to that, the precipitation finger structures show a clear pH difference of the fingers to the acidic solution in between. The strong precipitates act as a semipermeable mineral membrane that keeps high and low pH areas separated and, together with the continued inflow of OH^- ions, maintains the gradient even in the final state of the morphology. This can be clearly seen by the straight blue (alkaline) stripes in the cross-section versus time plot (Fig. 3B, right). Their width does not considerably vary over time, indicating a stable gradient between red (acidic) and blue (alkaline) areas. The maintenance of pH gradients across stable semipermeable membranes is a crucial feature for life as we know it today. The characteristic of pH gradient formation can only be observed for the precipitation fingers at mediate flow and concentration of inflowing fluid. Modern compartments, like cells, provide a similar setting: an alkaline interior separated by a membrane from an acidic surrounding. To keep the gradients across the membrane up, however, for cells mechanisms like transmembrane machines are needed to pump protons out of the cell (see fig. S2). In contrast, the finely finger-like structures in the microfluidic morphology would not require any active means or proton pumping as long as the flow of alkaline fluid continues.

Bead accumulation

The next step in testing the capabilities for compartmentalization is to check for potential accumulation of dissolved species in the fluids. We tested our different morphologies with fluorescent beads of 10 µm diameter. In Fig. 4, three experiments are shown with conditions yielding the dominant morphologies, but with dispersed fluorescent beads mixed in the inflowing fluid. It can be seen

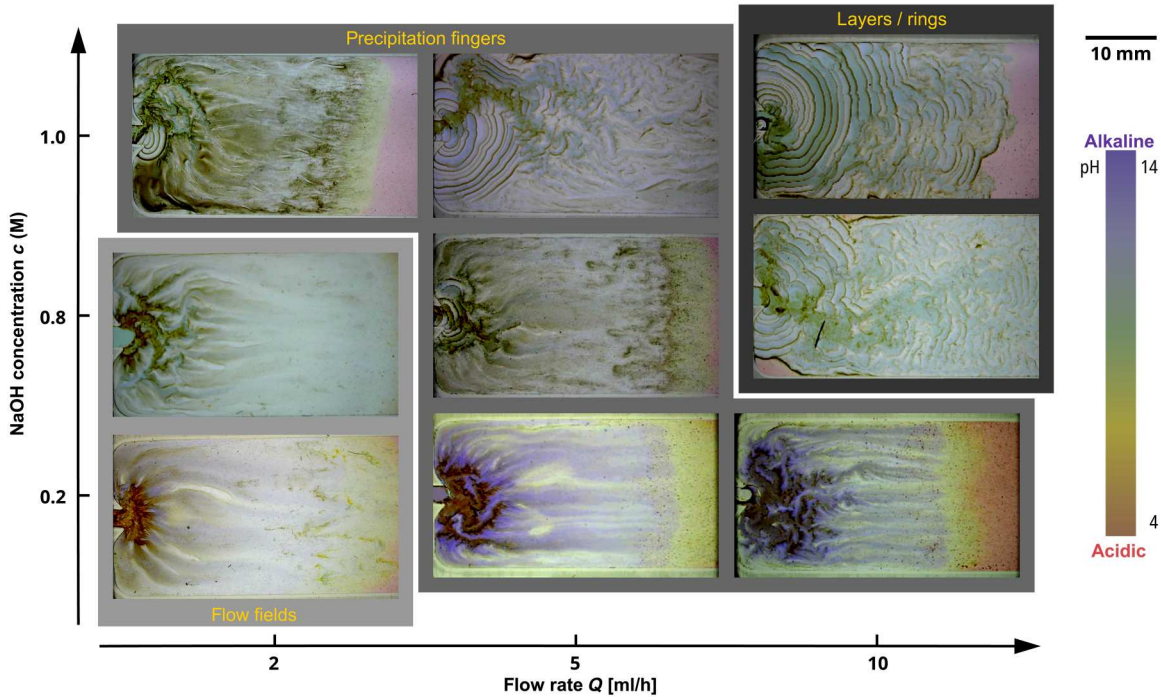

Fig. 2. Variation of inflow rate and concentration of the alkaline fluid. Injection of an NaOH solution into an ocean fluid containing 200 mM Fe(II)Cl_2 yields three dominant morphologies. Layers/rings form at high flow and concentrations, whereas diffusive fields persist at low values. In between both regimes, precipitate fingers form, which allow the formation and maintenance of steep pH gradients. At the higher limit, the acidic ocean is almost completely repressed by the precipitation front, and at the lower limit, both solution mix by diffusion due to weak precipitation. Therefore, no gradients can be formed or maintained in both limiting morphologies.

that beads are getting trapped inside the morphologies upon precipitation. In the flow fields (Fig. 4A), a very weak fluorescence signal indicates hardly any bead accumulation, which is most likely due to the weak precipitation and pH gradients. Although there appears to be a higher fluorescence signal in the layers/rings (Fig. 4C) due to their high inflow rate, most of the beads fade again over time as they are most likely flushed out. Nevertheless, beads are locally accumulated in some of the grooves along the fluid paths; however, they would not be subjected to any gradients or continued feeding after a shortcut flow forms after some time (see Fig. 3C). In the precipitation finger structures (Fig. 4B), we see that some beads are getting trapped in the precipitate upon formation, which forms local clusters of accumulated particles, increasing in fluorescence over time, which suggests continued accumulation over time as the influx persists. In this way, spots of locally increased concentration of accumulated particles form, which persist even after the precipitation process is finished.

DISCUSSION

Here, we showed that dominantly three different precipitation morphologies emerge in a quasi-2D AV model, which have different abilities to facilitate the emergence of pH gradients and accumulation of dispersed particles. In our studies, we identified flow rate and concentration of hydroxide ions (i.e., concentration of NaOH) in the inflowing fluid to be the critical parameters in structure formation and therefore focused on their variation in our experiments. Our data suggest that precipitation fingers, obtained at medium flow rates and medium concentrations of alkaline fluid within our boundaries, yield the steadiest gradients in terms of steepness and stability. Crucial for the formation of pH gradients is the subdivision of the flow into narrower "fingers" across the width of the chamber, which form strong mineral precipitates with the acidic solution in between. After reaching the morphological steady state, pH gradients are maintained by the continued inflow of hydroxide ions through all of the fingers. Although the layer/ring structures also exhibit strong precipitation barriers, they fail to generate gradients, since all of the ocean fluid is pushed out of the chamber by propagation of the precipitation front spanning across the whole chamber width (no acidic fluid enclosed). After some time, a main flow is established as a short cut through the morphologies, leading to fading fluorescence of the pH-dependent dye in the adjacent areas. This probably forms weak pH gradients between main flow and outer areas that are, however, not separated by a barrier. The lack of barriers seems also the problem for the flow fields as they hardly show any stable precipitate and therefore lack the ability to maintain gradients as the fluids just intermix through diffusion.

We observe that a change in the experimental parameters essentially corresponds to a shift of the morphology's formation timescale. This seems plausible, since precipitation happens more rapidly at higher concentrations and grows faster at higher flow rates. Therefore, we found that layers/rings form predominately within the first 20 s, then converge to the precipitation fingers between roughly 30 and 80 s, and finally fade into the diffusive fields after around 100 s as the local flow velocity ceases and diffusive movement dominates. In experiments exhibiting dominant precipitation fingers or flow fields, we can therefore observe small

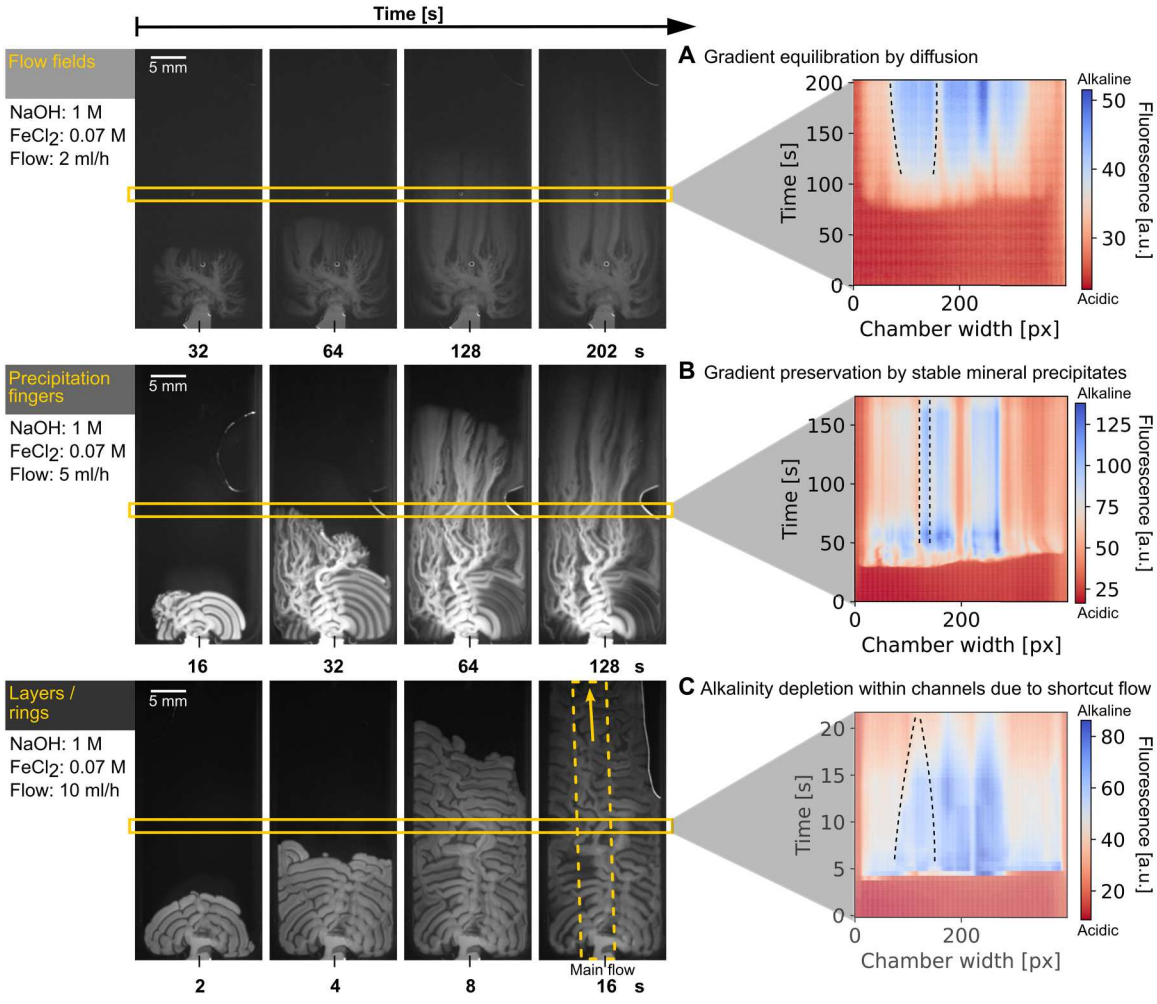

Fig. 3. Changes in inflow rate and concentration correspond to a timescale shift in morphology formation. Each of the three time series represents conditions that are dominated by one of the three morphologies. Layers/rings form predominately within the first 20 s, then converge to the finger structures between roughly 30 and 80 s, and finally fade into the flow fields after around 100 s. On the right, an average of 20 pixels in height over the cross-section of the chamber is plotted over time: (**A**) No steady state is reached and the fluids intermix by diffusion over time (blue areas become wider). (**B**) Stable gradients are formed between red (acidic) and blue (alkaline) areas and are maintained over time (straight blue stripes at persistent width). (**C**) In steady state, a dominant flow through the layers forms and fluorescence fades in adjacent structures, indicated by narrowing of the blue (alkaline) areas.

sections of the other two morphologies at the respective timescale. To promote the formation of gradients, precipitation fingers should be extended as far as possible, which works best by ensuring stable precipitates using medium to high OH^- concentration and medium flow rates.

In the experiments with fluorescent beads mixed into the inflowing solution, accumulation could only be deduced in the parallel precipitation finger structures and the layers/rings, which can be seen by the increasing fluorescence intensity of the agglomerates. While some of the beads are already trapped during the mineral precipitation process, more are accumulated as long as the inflow continues. This could be due to diffusiophoretic effects (*9*) or the advective flows through the resulting structures. However, in the layers/rings, the beads only seem to increase in the grooves and are thus not subject to either gradients or the continued inflow, after the shortcut flow establishes.

In the field of chemobrionics, confined quasi-2D flow setups (Hele-Shaw flow cells) are commonly used to study precipitation reactions and the resulting pattern formation. The experiments mostly use radial injection of the fluid (*10*, *41*, *42*, *45*–*47*) rather than injection from one side as in our setting. Although we used different injections and chemical compositions, Rocha *et al.* (*46*) showed the formation of similar morphologies over the time of the experiment. However, none of the patterns identified in the referenced literature coincides exactly with our dominant morphologies, which would make our setting also interesting for modeling of the pattern formation process.

Modern AV systems, such as Lost City, can be seen as an example to our model by structure, but not by chemical composition. We selected the fluids to resemble the crucial conditions that allow the precipitation of minerals upon contact and are assumed to have been prevalent on an early Earth. Although we did not aim to recreate the formation of any specific minerals, it is likely that

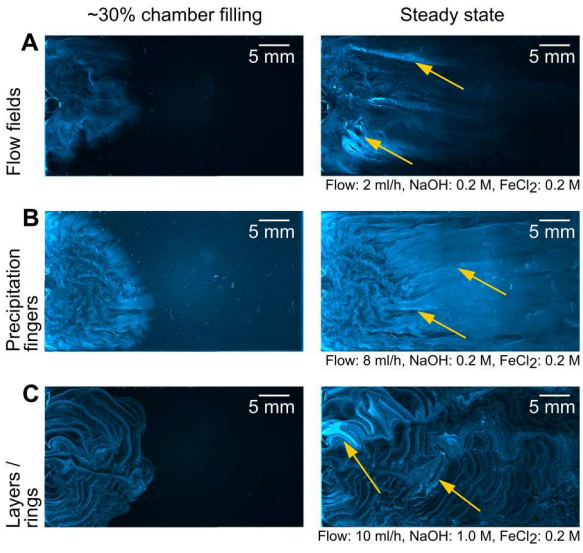

Fig. 4. Accumulation of fluorescent beads in the different dominant morphologies. Ten-micrometer fluorescent beads are dispersed into the alkaline fluid to visualize accumulation in layers/rings (**A**), precipitation fingers (**B**), and flow fields (**C**). Strongest local increase of fluorescence is observed in the precipitation fingers (B), suggesting the accumulation of dispersed beads.

we create white and green rust (amakinite and fougerite) as shown in previous work under comparable conditions (*15*). Although Lost City is considered a low-temperature AV system, the vented fluids still have temperatures 40° to 75°C (*24*, *25*). Our results presented here were mainly focused on experiments carried out at room temperature, but as fig. S3 shows, the injection of heated fluids seems not to have any notable influence on the resulting morphologies. Our setup forms the technical basis to test many other geochemical reagents in a microfluidic setting, which would, however, exceed the scope of this paper. Particularly interesting would be the integration of carbonate as occurring in modern Lost City–type vents (*24*, *25*) and sulfide. Both of them were also likely abundant on an early Earth (*1*–*3*) and are even providing promising catalytic capabilities known from highly reactive metal sulfides like Fe(Ni)S minerals (*23*, *52*–*54*). So far, sulfides were not included in the system due to safety reason and the potential formation of H_2S gas. Future experiments may not only involve further reagents but also aim to sufficiently extract the formed precipitates from the microfluidic cell and subsequent analysis with Raman spectroscopy or scanning electron microscopy (*15*).

Our setup allows to study the AV formation process in quasi–two dimensions, thereby providing full optical access for fluorescence and bright-field visualization and allowing for the precise control of chamber thickness and inflow rate. All previous attempts to recreate the AV formation process in the laboratory were focused on a 3D setup (*23*, *37*). Because of technical limitations of our microscope, the flow cell could only be located horizontally in our experiments, but given the close density values of the fluids (table S1), buoyancy effect would be negligible. The 2D representation serves as a model for the precipitation process in 3D and only requires sample volumes lower than 100 μl. As the AV precipitates provide highly reactive mineral surfaces (*13*, *15*), this would also provide a promising setting to study the effect of minerals and gradients on origins of life–related chemical reactions in low volumes. Apart from that, the confined geometry could probably be seen not only as a model but also as a potential geological scenario, considering the possibility that the vent precipitation process could already start in the cracks of the crust before the fluids are exhaled into the bulk ocean waters.

From an origins of life perspective, the quasi-2D scenario could satisfy several requirements, which are thought to be crucial for the emergence of living systems. Essentially, all life we know today depends on nonequilibria and, thus, requires gradients of ions and pH that are separated by a semipermeable membrane (*9*). In the alkaline hydrothermal vent theory, it is therefore considered that geochemical gradients could pose an early precursor to the topology of living systems, given their structural similarities to autotrophic cells (*3*, *9*). This is also clearly reflected in our precipitation finger morphology, with the alkaline fluid streaming inside the finger structures, which are separated by a thin mineral barrier from the more acidic ocean solution in between the streams.

In order for chemical reactions to happen and to start molecular evolution, it requires high concentration of molecules and means to localize reagents and products to avoid dilution in an extensive ocean, an issue usually referred to as the "concentration problem" (*55*). Via diffusiophoresis, the ion gradients could facilitate a directed colloid transport (*9*) in addition to the trapping of dissolved species in the physical structure of the morphologies (e.g., formed pockets) to even further boost the accumulation of (macro-)molecules. Further, accumulation could be aided by thermophoresis due to temperature gradients between the two fluids (*56*). This would enhance the local concentration of dissolved molecules, which in turn could be localized by trapping or interaction with the minerals (*15*) and eventually participate in reactions catalyzed by the minerals. Further experiments will also consider 2D matrix-assisted laser desorption/ionization (MALDI) imaging of the dried precipitates to map out local accumulation sites of different organic molecules within the mineral structures.

Theoretical ideas also suggest that steep proton gradients across the thin mineral membranes in AVs could facilitate CO_2 reduction that enables abiotic organic syntheses similar to the acetyl–coenzyme A pathway in bacteria and archea (*3*, *23*, *57*). Recent experimental work (*21*–*23*), however, has shown only very low yields of simple organic products so far. Also, because of that, electrochemical gradients in AVs may pose an important role by combining strongly opposing conditions (high-low pH or reduced-oxidized) for different or subsequent chemical reactions (*13*) in close spatial proximity and driving diffusiophoretic accumulation of dilute molecules (*9*) at catalytically active mineral surfaces (*3*, *9*, *14*). The catalytic potential of different iron sulfide minerals has been shown in recent experimental publications for the reduction of CO_2 (*53*, *54*, *58*) and also the effect of oxyhydroxide minerals on product selectivity in amino acid synthesis (*13*).

We investigated the precipitation of hydrothermal vent morphologies in a quasi-2D setting. We found that finger-like precipitates at medium flow rate and OH^- concentration allow for the generation and maintenance of pH gradients and facilitate the accumulation of dispersed particles at the same time. Considering the possibility that AV precipitation could already happen within the fractures of the seafloor, the confined geometry could even be a promising mimic of geological scenario. Our microfluidic setup allows the spatiotemporal visualization of the precipitation

process and the emerging gradients with universal and fluorescent pH dyes. This could open the door for laboratory experiments in low volume to study the impact of AV environments on accumulation of organic molecules, catalytic reactions, and processes like polymerization or replication of biopolymers.

MATERIALS AND METHODS

The microfluidic setup (fig. S1A) is a custom-made flow cell consisting of a 2D rectangular geometry (16 mm × 40 mm) with inlet/outlet channels (fig. S1C) cut out of a 500-μm-thick sheet of fluorinated ethylene propylene (FEP). To form a closed chamber, the sheet is sandwiched between two transparent sapphire plates of size 22 mm × 60 mm with a thickness of 1.0 mm (top) and 0.5 mm (bottom). The three layers are pressed together by a steel frame screwed on an aluminum base to tightly seal the chamber. Hydrodynamic access to the chamber is provided by a total of four holes in the thin bottom sapphire that are connected to polytetrafluoroethylene (PTFE) tubings (inside diameter, 180 μm) via standard low-pressure fittings, ferrules, and corresponding threads in the aluminum base.

Microscopy and visualization

For visualization of the chamber′s interior, the setup is placed on the stage of a microscope (Axio Zoom.V16, Carl Zeiss, Germany) using a 3D-printed support frame. For bright-field imaging, the chamber is illuminated by the microscope′s built-in white light source from below, whereas for fluorescence imaging the sample is excited from above by the white light from a light engine (SOLA 80-10247, Lumencor, USA) coupled with a Zeiss 38 He filter to generate a 470/40-mm light through the objective lens (0.5×). Images are recorded using a complementary metal-oxide semiconductor (CMOS) camera (ORCA-Flash 4.0, Hamamatsu, Japan) or a mirrorless photographic camera (Lumix DC-G100K, Panasonic, Japan) for color imaging mounted to the microscope with a C-mount adapter.

Microfluidics

The chamber is prefilled manually with the ocean analog, whereas injection of the alkaline fluid is controlled by a pulsation-free, continuous-flow syringe pump (Nemesys S, Cetoni, Germany) operated with glass syringes (1 ml) at varying flow rates of 1.0 to 15.0 ml hour^{-1}.

The FEP cutout (fig. S1C) features channels of 1.7 mm width that connect the rectangular cell to the holes in the sapphire. In preparation of the experiment, the chamber is prefilled with ocean analog solution through the top outlet channels while keeping the inlet channels closed to avoid precipitation happening in the channels. To avoid bubbles in the chamber, the alkaline solution is slowly pumped into the inlet channel (2 ml hour^{-1}) while simultaneously retrieving the air through the drainage channel at the same rate. All motion is stopped when the fluid front is 2 mm from entering the chamber, the drainage channel is closed, and the experiment is started at the desired flow rate.

Sample preparation

The acidic ocean analog is prepared by dissolving iron(II)chloride tetrahydrate [Fe(II)$Cl_2 \cdot 4H_2O$] (Sigma-Aldrich, USA) in nuclease-free water (Ambion, Invitrogen, Thermo Fisher Scientific, USA) to reach concentrations of either 75 or 200 mM. To keep oxidation of the solution to a minimum, iron(II)chloride tetrahydrate is stored under inert gas (argon) and all flasks and vials are preflushed with argon gas. As alkaline fluid, a commercial volumetric standard solution of sodium hydroxide [NaOH] (Carl Roth, Germany) is either used as purchased (1 M) or diluted with nuclease-free water to reach the desired concentration. Depending on the experiment, the fluids are used directly, mixed in a ratio of 8:1 with a universal pH dye (KS90-UpHI, Lovibond, Tintometer, Germany), or mixed 50:1 with a solution of BCECF (Invitrogen, Thermo Fisher Scientific, USA) for fluorescent imaging. For visualization of fluid flow and particle accumulation, the inflowing sodium hydroxide solution was mixed in a ratio of 18:1 with a 2.5% aqueous suspension of 10-μm fluorescent (bright blue) carboxylate polystyrene microspheres (Fluoresbrite, Polysciences, USA).

Supplementary Materials

This PDF file includes:
Figs. S1 to S4
Table S1
Legends for movies S1 to S9

Other Supplementary Material for this manuscript includes the following:
Movies S1 to S9

REFERENCES AND NOTES

1. M. J. Russell, A. J. Hall, The emergence of life from iron monosulphide bubbles at a submarine hydrothermal redox and pH front. *J. Geol. Soc. London* **154**, 377–402 (1997).
2. W. Martin, J. Baross, D. Kelley, M. J. Russell, Hydrothermal vents and the origin of life. *Nat. Rev. Microbiol.* **6**, 805–814 (2008).
3. V. Sojo, B. Herschy, A. Whicher, E. Camprubí, N. Lane, The origin of life in alkaline hydrothermal vents. *Astrobiology* **16**, 181–197 (2016).
4. N. G. Holm, Why are hydrothermal systems proposed as plausible environments for the origin of life?, in *Marine Hydrothermal Systems and the Origin of Life* (Springer Netherlands, 1992), pp. 5–14.
5. S. W. Poulton, D. E. Canfeld, Ferruginous conditions: A dominant feature of the ocean through Earth′s history. *Elements* **7**, 107–112 (2011).
6. E. G. Nisbet, The geological setting of the earliest life forms. *J. Mol. Evol.* **21**, 289–298 (1985).
7. M. Preiner, J. C. Xavier, F. L. Sousa, V. Zimorski, A. Neubeck, S. Q. Lang, H. Chris Greenwell, K. Kleinermanns, H. Tüysüz, T. M. McCollom, N. G. Holm, W. F. Martin, Serpentinization: Connecting geochemistry, ancient metabolism and industrial hydrogenation. *Life* **8**, 41 (2018).
8. M. J. Russell, A. J. Hall, W. Martin, Serpentinization as a source of energy at the origin of life. *Geobiology* **8**, 355–371 (2010).
9. F. M. Möller, F. Kriegel, M. Kieß, V. Sojo, D. Braun, Steep pH gradients and directed colloid transport in a microfluidic alkaline hydrothermal pore. *Angew. Chem. Int. Ed.* **56**, 2340–2344 (2017).
10. Q. Wang, K. S. Hernesman, O. Steinbock, Flow-driven precipitation patterns with microemulsions in a confined geometry. *ChemSystemsChem* **2**, e1900037 (2020).
11. C. F. Dirscherl, A. Ianeselli, D. Tetiker, T. Matreux, R. M. Queener, C. B. Mast, D. Braun, A heated rock crack captures and polymerizes primordial DNA and RNA. *Phys. Chem. Chem. Phys.* **25**, 3375–3386 (2023).
12. T. Matreux, B. Altaner, J. Raith, D. Braun, C. B. Mast, U. Gerland, Formation mechanism of thermally controlled ph gradients. *Commun. Phys.* **6**, 14 (2023).
13. L. M. Barge, E. Flores, M. M. Baum, D. G. Velde, M. J. Russell, Redox and pH gradients drive amino acid synthesis in iron oxyhydroxide mineral systems. *Proc. Natl. Acad. Sci. U.S.A.* **116**, 4828–4833 (2019).
14. N. H. Sleep, A. Meibom, T. Fridriksson, R. G. Coleman, D. K. Bird, H2-rich fluids from serpentinization: Geochemical and biotic implications. *Proc. Natl. Acad. Sci. U.S.A.* **101**, 12818–12823 (2004).
15. V. Helmbrecht, M. Weingart, F. Klein, D. Braun, W. D. Orsi, White and green rust chimneys accumulate RNA in a ferruginous chemical garden. arXiv:2212.02793 [physics.geo-ph] (6 December 2022).

16. S. Duhr, D. Braun, Why molecules move along a temperature gradient. *Proc. Natl. Acad. Sci. U.S.A.* **103**, 19678–19682 (2006).
17. P. Baaske, F. M. Weinert, S. Duhr, K. H. Lemke, M. J. Russell, D. Braun, Extreme accumulation of nucleotides in simulated hydrothermal pore systems. *Proc. Natl. Acad. Sci. U.S.A.* **104**, 9346–9351 (2007).
18. A. V. Dass, S. Wunnava, J. Langlais, B. von der Esch, M. Krusche, L. Ufer, N. Chrisam, R. C. A. Dubini, F. Gartner, S. Angerpointner, C. F. Dirscherl, P. Rovó, C. B. Mast, J. E. Šponer, C. Ochsenfeld, E. Frey, D. Braun, RNA oligomerisation without added catalyst from 2′,3′-cyclic nucleotides by drying at air-water interfaces. *ChemSystemsChem* **5**, e202200026 (2023).
19. C. B. Mast, D. Braun, Thermal trap for DNA replication. *Phys. Rev. Lett.* **104**, 188102 (2010).
20. C. B. Mast, S. Schink, U. Gerland, D. Braun, Escalation of polymerization in a thermal gradient. *Proc. Natl. Acad. Sci. U.S.A.* **110**, 8030–8035 (2013).
21. V. Sojo, A. Ohno, S. E. McGlynn, Y. M. A. Yamada, R. Nakamura, Microfluidic reactors for carbon fixation under ambient-pressure alkaline-hydrothermal-vent conditions. *Life* **9**, 16 (2019).
22. R. Hudson, R. de Graaf, M. S. Rodin, A. Ohno, N. Lane, S. E. McGlynn, Y. M. A. Yamada, R. Nakamura, L. M. Barge, D. Braun, V. Sojo, CO_2 reduction driven by a pH gradient. *Proc. Natl. Acad. Sci. U.S.A.* **117**, 22873–22879 (2020).
23. B. Herschy, A. Whicher, E. Camprubi, C. Watson, L. Dartnell, J. Ward, J. R. G. Evans, N. Lane, An origin-of-life reactor to simulate alkaline hydrothermal vents. *J. Mol. Evol.* **79**, 213–227 (2014).
24. D. S. Kelley, J. A. Karson, D. K. Blackman, G. L. Früh-Green, D. A. Butterfield, M. D. Lilley, E. J. Olson, M. O. Schrenk, K. K. Roe, G. T. Lebon, P. Rivizzigno; AT3-60 Shipboard Party, An off-axis hydrothermal vent field near the Mid-Atlantic Ridge at 30° N. *Nature* **412**, 145–149 (2001).
25. D. S. Kelley, J. A. Karson, G. L. Früh-Green, D. R. Yoerger, T. M. Shank, D. A. Butterfield, J. M. Hayes, M. O. Schrenk, E. J. Olson, G. Proskurowski, M. Jakuba, A. Bradley, B. Larson, K. Ludwig, D. Glickson, K. Buckman, A. S. Bradley, W. J. Brazelton, K. Roe, M. J. Elend, A. Delacour, S. M. Bernasconi, M. D. Lilley, J. A. Baross, R. E. Summons, S. P. Sylva, A serpentinite-hosted ecosystem: The Lost City hydrothermal field. *Science* **307**, 1428–1434 (2005).
26. W. Bach, H. Paulick, C. J. Garrido, B. Ildefonse, W. P. Meurer, S. E. Humphris, Unraveling the sequence of serpentinization reactions: Petrography, mineral chemistry, and petrophysics of serpentinites from MAR 15°N (ODP Leg 209, Site 1274). *Geophys. Res. Lett.* **33**, (2006).
27. G. Macleod, C. McKeown, A. J. Hall, M. J. Russell, Hydrothermal and oceanic pH conditions of possible relevance to the origin of life. *Orig. Life Evol. Biosph.* **24**, 19–41 (1994).
28. I. Halevy, A. Bachan, The geologic history of seawater pH. *Science* **355**, 1069–1071 (2017).
29. E. D. Swanner, N. Lambrecht, C. Wittkop, C. Harding, S. Katsev, J. Torgeson, S. W. Poulton, The biogeochemistry of ferruginous lakes and past ferruginous oceans. *Earth Sci. Rev.* **211**, 103430 (2020).
30. T. Altair, L. G. F. Borges, D. Galante, H. Varela, Experimental approaches for testing the hypothesis of the emergence of life at submarine alkaline vents. *Life* **11**, 777 (2021).
31. U. Pedreira-Segade, C. Feuillie, M. Pelletier, L. J. Michot, I. Daniel, Adsorption of nucleotides onto ferromagnesian phyllosilicates: Significance for the origin of life. *Geochim. Cosmochim. Acta* **176**, 81–95 (2016).
32. J. S. Beard, B. R. Frost, P. Fryer, A. McCaig, R. Searle, B. Ildefonse, P. Zinin, S. K. Sharma, Onset and progression of serpentinization and magnetite formation in olivine-rich troctolite from IODP Hole U1309D. *J. Petrol.* **50**, 387–403 (2009).
33. F. Trolard, S. Duval, W. Nitschke, B. Ménez, C. Pisapia, J. Ben Nacib, M. Andréani, G. Bourrié, Mineralogy, geochemistry and occurrences of fougerite in a modern hydrothermal system and its implications for the origin of life. *Earth Sci. Rev.* **225**, 103910 (2022).
34. S. E. McGlynn, I. Kanik, M. J. Russell, Peptide and RNA contributions to iron-sulphur chemical gardens as life's first inorganic compartments, catalysts, capacitors and condensers. *Philos. Trans. R. Soc. A Math. Phys. Eng. Sci.* **370**, 3007–3022 (2012).
35. L. M. Barge, Y. Abedian, I. J. Doloboff, J. E. Nuñez, M. J. Russell, R. D. Kidd, I. Kanik, Chemical gardens as flow-through reactors simulating natural hydrothermal systems. *J. Vis. Exp.* **2015**, 53015 (2015).
36. B. T. Burcar, L. M. Barge, D. Trail, E. B. Watson, M. J. Russell, L. B. McGown, RNA oligomerization in laboratory analogues of alkaline hydrothermal vent systems. *Astrobiology* **15**, 509–522 (2015).
37. L. M. Barge, S. S. S. Cardoso, J. H. E. Cartwright, G. J. T. Cooper, L. Cronin, A. De Wit, I. J. Doloboff, B. Escribano, R. E. Goldstein, F. Haudin, D. E. H. Jones, A. L. Mackay, J. Maselko, J. J. Pagano, J. Pantaleone, M. J. Russell, C. I. Sainz-Díaz, O. Steinbock, D. A. Stone, Y. Tanimoto, N. L. Thomas, From chemical gardens to chemobrionics. *Chem. Rev.* **115**, 8652–8703 (2015).
38. J. H. E. Cartwright, J. M. García-Ruiz, M. L. Novella, F. Otálora, Formation of chemical gardens. *J. Colloid Interface Sci.* **256**, 351–359 (2002).
39. D. A. Stone, B. Lewellyn, J. C. Baygents, R. E. Goldstein, Precipitative growth templated by a fluid jet. *Langmuir* **21**, 10916–10919 (2005).
40. F. Haudin, J. H. E. Cartwright, F. Brau, A. De Wit, Spiral precipitation patterns in confined chemical gardens. *Proc. Natl. Acad. Sci. U.S.A.* **111**, 17363–17367 (2014).
41. E. Balog, P. Papp, Á. Tóth, D. Horváth, G. Schuszter, The impact of reaction rate on the formation of flow-driven confined precipitate patterns. *Phys. Chem. Chem. Phys.* **22**, 13390–13397 (2020).
42. K. V. Bere, E. Nez, E. Balog, L. Janovák, D. Sebők, Á. Kukovecz, C. Roux, V. Pimienta, G. Schuszter, Enhancing the yield of calcium carbonate precipitation by obstacles in laminar flow in a confined geometry. *Phys. Chem. Chem. Phys.* **23**, 15515–15521 (2021).
43. C. I. Sainz-Díaz, E. Escamilla-Roa, J. H. E. Cartwright, Growth of self-assembling tubular structures of magnesium oxy/hydroxide and silicate related with seafloor hydrothermal systems driven by serpentinization. *Geochem. Geophys. Geosyst.* **19**, 2813–2822 (2018).
44. Y. Ding, C. M. Gutiérrez-Ariza, M. Zheng, A. Felgate, A. Lawes, C. I. Sainz-Díaz, J. H. E. Cartwright, S. S. S. Cardoso, Downward fingering accompanies upward tube growth in a chemical garden grown in a vertical confined geometry. *Phys. Chem. Chem. Phys.* **24**, 17841–17851 (2022).
45. G. Schuszter, F. Brau, A. De Wit, Flow-driven control of calcium carbonate precipitation patterns in a confined geometry. *Phys. Chem. Chem. Phys.* **18**, 25592–25600 (2016).
46. L. A. M. Rocha, L. Thorne, J. J. Wong, J. H. E. Cartwright, S. S. S. Cardoso, Archimedean spirals form at low flow rates in confined chemical gardens. *Langmuir* **38**, 6700–6710 (2022).
47. A. Comolli, A. De Wit, F. Brau, Dynamics of $A + B \rightarrow C$ reaction fronts under radial advection in a Poiseuille flow. *Phys. Rev. E* **104**, 044206 (2021).
48. S. Leduc, *The Mechanism of Life* (Rebman, 1911).
49. Q. Wang, O. Steinbock, Materials synthesis and catalysis in microfluidic devices: Prebiotic chemistry in mineral membranes. *ChemCatChem* **12**, 63–74 (2020).
50. B. C. Batista, O. Steinbock, Growing inorganic membranes in microfluidic devices: Chemical gardens reduced to linear walls. *J. Phys. Chem. C* **119**, 27045–27052 (2015).
51. Q. Wang, L. M. Barge, O. Steinbock, Microfluidic production of pyrophosphate catalyzed by mineral membranes with steep pH gradients. *Chemistry* **25**, 4732–4739 (2019).
52. L. M. White, R. Bhartia, G. D. Stucky, I. Kanik, M. J. Russell, Mackinawite and greigite in ancient alkaline hydrothermal chimneys: Identifying potential key catalysts for emergent life. *Earth Planet. Sci. Lett.* **430**, 105–114 (2015).
53. T. Beyazay, K. S. Belthle, C. Farès, M. Preiner, J. Moran, W. F. Martin, H. Tüysüz, Ambient temperature CO_2 fixation to pyruvate and subsequently to citramalate over iron and nickel nanoparticles. *Nat. Commun.* **14**, 570 (2023).
54. T. Beyazay, C. Ochoa-Hernández, Y. Song, K. S. Belthle, W. F. Martin, H. Tüysüz, Influence of composition of nickel-iron nanoparticles for abiotic CO_2 conversion to early prebiotic organics. *Angew. Chem. Int. Ed.* **62**, e202218189 (2023).
55. C. De Duve, R. De Neufville, *Blueprint for a Cell: The Nature and Origin of Life* (Carolina Biological Supply Company, 1991).
56. L. Keil, M. Hartmann, S. Lanzmich, D. Braun, Probing of molecular replication and accumulation in shallow heat gradients through numerical simulations. *Phys. Chem. Chem. Phys.* **18**, 20153–20159 (2016).
57. A. Yamaguchi, M. Yamamoto, K. Takai, T. Ishii, K. Hashimoto, R. Nakamura, Electrochemical CO_2 reduction by Ni-containing iron sulfides: How is CO_2 electrochemically reduced at bisulfide-bearing deep-sea hydrothermal precipitates? *Electrochim. Acta* **141**, 311–318 (2014).
58. M. Preiner, K. Igarashi, K. B. Muchowska, M. Yu, S. J. Varma, K. Kleinermanns, M. K. Nobu, Y. Kamagata, H. Tüysüz, J. Moran, W. F. Martin, A hydrogen-dependent geochemical analogue of primordial carbon and energy metabolism. *Nat. Ecol. Evol.* **4**, 534–542 (2020).

Acknowledgments: We thank L. S. Gigou for assistance in preliminary experiments, A. Schmid and C. F. Dirscherl for extensive comments on figures and manuscript, and J. H. Cartwright for comments on data and manuscript. **Funding:** This work was supported by the European Research Council (ERC) Evotrap, grant no. 787356 (D.B.); the Deutsche Forschungsgemeinschaft (DFG, German Research Foundation)—Project-ID 364653263—TRR 235 (CRC 235) (D.B. and W.D.O.); and the Max Planck Society (K.A.). **Author contributions:** M.W., D.B., and K.A. designed the experiments. M.W., C.D., and S.C. performed all experiments. V.H. and W.D.O. developed the sample composition and gave major input on geological interpretation. M.W., S.C., V.H., W.D.O., and K.A. analyzed the data. K.A. and D.B. supervised the project. M.W. wrote the manuscript, and all authors commented on the manuscript and contributed to the writing process. All authors edited and reviewed the manuscript for resubmission. **Competing interests:** The authors declare that they have no competing interests. **Data and materials availability:** All data needed to evaluate the conclusions in the paper are present in the paper and/or the Supplementary Materials. The collected experimental data are openly available in the mediaTUM repository under URL/DOI: doi.org/10.14459/2023mp1716502.

Submitted 24 April 2023
Accepted 30 August 2023
Published 29 September 2023
10.1126/sciadv.adi1884

ScienceAdvances

Alkaline vents recreated in two dimensions to study pH gradients, precipitation morphology, and molecule accumulation

Maximilian Weingart, Siyu Chen, Clara Donat, Vanessa Helmbrecht, William D. Orsi, Dieter Braun, and Karen Alim

Sci. Adv. **9** (39), eadi1884. DOI: 10.1126/sciadv.adi1884

Science Advances (ISSN 2375-2548) is published by the American Association for the Advancement of Science. 1200 New York Avenue NW, Washington, DC 20005. The title *Science Advances* is a registered trademark of AAAS.